AGU PUBLICATIONS

Geophysical Research Letters

RESEARCH LETTER
10.1002/2017GL073114

Special Section:
Early Results: Juno at Jupiter

Morphology of the UV aurorae Jupiter during Juno's first perijove observations

B. Bonfond[1], G. R. Gladstone[2], D. Grodent[1], T. K. Greathouse[2], M. H. Versteeg[2], V. Hue[2], M. W. Davis[2], M. F. Vogt[3], J.-C. Gérard[1], A. Radioti[1], S. Bolton[2], S. M. Levin[4], J. E. P. Connerney[5], B. H. Mauk[6], P. Valek[2], A. Adriani[7], and W. S. Kurth[8]

[1]Space sciences, Technologies and Astrophysics Research (STAR) Institute, LPAP, Université de Liège, Liège, Belgium, [2]Southwest Research Institute, San Antonio, Texas, USA, [3]Center for Space Physics, Boston University, Boston, Massachusetts, USA, [4]Jet Propulsion Laboratory, Pasadena, California, USA, [5]Goddard Space Flight Center, Greenbelt, Maryland, USA, [6]The Johns Hopkins University Applied Physics Laboratory, Laurel, Maryland, USA, [7]INAF-IAPS, Rome, Italy, [8]Department of Physics and Astronomy, University of Iowa, Iowa City, Iowa, USA

Abstract On 27 August 2016, the NASA Juno spacecraft performed its first close-up observations of Jupiter during its perijove. Here we present the UV images and color ratio maps from the Juno-UVS UV imaging spectrograph acquired at that time. Data were acquired during four sequences (three in the north, one in the south) from 5:00 UT to 13:00 UT. From these observations, we produced complete maps of the Jovian aurorae, including the nightside. The sequence shows the development of intense outer emission outside the main oval, first in a localized region (255°–295° System III longitude) and then all around the pole, followed by a large nightside protrusion of auroral emissions from the main emission into the polar region. Some localized features show signs of differential drift with energy, typical of plasma injections in the middle magnetosphere. Finally, the color-ratio map in the north shows a well-defined area in the polar region possibly linked to the polar cap.

Key Points:
- During Perijove 1, Juno-UVS acquired the first spatially and spectrally resolved Far-UV observations of Jupiter's nightside aurorae
- During the 10 h sequences, large and intense outer emissions progressively developed and a protrusion formed with the southern main oval
- A well-defined area identified in the northern polar region resembles the shape, location, and area of the predicted open field line region

Supporting Information:
- Supporting Information S1
- Movie S1

Correspondence to:
B. Bonfond,
b.bonfond@ulg.ac.be

Citation:
Bonfond, B., et al. (2017), Morphology of the UV aurorae Jupiter during Juno's first perijove observations, *Geophys. Res. Lett.*, *44*, doi:10.1002/2017GL073114.

Received 16 FEB 2017
Accepted 26 MAR 2017

1. Introduction

The UV aurorae of Jupiter are made of multiple components arising from different processes within the magnetosphere [*Grodent*, 2015]. The satellite footprints arise from the interaction between either Io, Europa, or Ganymede and the magnetospheric plasma rotating around the planet (see review in *Bonfond* [2012] and *Connerney et al.* [1993]). In the same region as the footprints are diffuse emissions related to the pitch angle diffusion boundary between dipolar and stretched field lines [*Radioti et al.*, 2009], as well as more compact structures associated with injections of hot and low-density plasma from the middle magnetosphere (10–40 Jovian radii (R_J)) into the inner magnetosphere (<10 R_J) [*Mauk et al.*, 2002; *Dumont et al.*, 2014; *Gray et al.*, 2016]. All together these features form the outer emissions, since they are located outside the most remarkable feature of the Jovian aurorae, called the main emission (or main oval). The main emission is associated with the upward branch of the corotation enforcement currents in the middle magnetosphere [*Hill*, 2001; *Cowley and Bunce*, 2001]. It is made of quasi-continuous curtains of emission with a dimmer portion in the prenoon sector, called the discontinuity [*Grodent et al.*, 2003a; *Radioti et al.*, 2008a]. The dusk sector of the main emission is occasionally very disturbed and pushed poleward, most likely in response to the arrival of a solar wind disturbance [*Nichols et al.*, 2007]. The shape of the main emission is essentially fixed in System III (S_{III}), the longitude system related to the magnetic field of Jupiter. Expansions of the main emission over weeks as well as increased occurrence rates of intense outer emissions have been tentatively associated with either magnetosphere expansion or internally driven increased outward transport that could be related or not to enhanced volcanism at Io [*Bonfond et al.*, 2012; *Badman et al.*, 2016]. Inside the main emission are the polar emissions, which can themselves be subdivided into three main regions: (1) the dark region, on the dawn flank, which is essentially devoid of emission; (2) the active region, on the duskside, which is a complex mixture of arcs, patches, and diffuse emissions; and finally, (3) the swirl region, peppered with chaotic patches of auroral emission [*Grodent et al.*, 2003b]. Transient (a few tens of minutes) spots and short arcs are regularly seen inside the dawn and midnight flanks of the main emission. Called either midnight or polar dawn spots, these features have been associated with signatures of recent reconnection related to the Vasyliunas cycle

[*Grodent et al.*, 2003b; *Radioti et al.*, 2008b]. Narrow, long-lived (> 1 h) and quasi-Sun-aligned polar auroral filaments (PAFs) are also often seen across the swirl region [*Nichols et al.*, 2009]. Finally, short-lived (~1 min) but intense features, called flares, are often observed in the active region [*Waite et al.*, 2001]. In half of the cases, such flares produce a quasiperiodic behavior in timescales of 2–3 min [*Bonfond et al.*, 2011, 2016].

This brief description is predominantly based on observations from the Earth-orbiting Hubble Space Telescope (HST). Unfortunately, the HST observing geometry is restricted to the Jovian longitudes facing the Sun and only offers limited views of the aurorae seen from the side. Even worse, the inclination of the magnetic dipole compared to the rotation axis induces a selection bias in addition to the local time bias, since most HST observations favored geometries where the magnetic pole of interest is tilted toward the observer. For the first time, Juno's unique vantage point from polar orbit provides us with the opportunity to view the Jovian aurorae entirely, from dusk to dawn and from noon to midnight. Here we describe the findings from the UV imaging spectrograph observations acquired on 27 August 2016, during the first perijove (PJ1) after Juno's orbit insertion.

2. Juno-UVS Auroral Observations

Juno is a spin-stabilized spacecraft orbiting Jupiter on an elongated 53.5 day polar orbit. On 27 August 2016, during its first perijove (PJ1) since orbit insertion, its spin and orbital planes were both nearly perpendicular to the Earth direction. Seen from the Earth, Juno travels clockwise around the planet while it spins counterclockwise twice per minute. The Juno-UVS (ultraviolet spectrograph) instrument is a UV photon-counting imaging spectrograph operating in the 68 to 210 nm range [*Gladstone et al.*, 2014; *Greathouse et al.*, 2013; *Davis et al.*, 2011]. It is equipped with a scan mirror that allows it to look up to ±30° perpendicular to the Juno spin plane. The slit's long axis is parallel to the spin axis. The "dog bone"-shaped slit is made of three segments with fields of view of 0.2° × 2.55°, 0.025° × 2.0°, and 0.2° × 2.55° projected onto the sky. The data from the instrument consist of a list of photon detection events with *X* position of the count on the detector corresponding to the spectral dimension and the *Y* position to the spatial dimension along the slit. Images can then be reconstructed by taking advantage of the motion of the field of view across the planet. The outcome is a stripe that covers an increasingly smaller part of the aurorae as Juno approaches Jupiter. The commanded position of the scan mirror allows the targeting of different regions of the aurorae. These successive stripes acquired every ~30 s can then be projected on polar maps and even coadded to get a complete picture of the aurorae at high spatial resolution. In the figures presented below, the projection altitude has been set to 400 km above the 1 bar level [*Bonfond et al.*, 2015]. The conversion from counts to kilo-Rayleighs depends on the effective area determined during the cruise period to Jupiter. The temporal variability of the effective area may induce an uncertainty of a factor of 2, and a calibration effort is still ongoing at this early stage of the mission. The brightness provided in this paper corresponds to the total brightness emitted by H_2 in the whole EUV+FUV range. It corresponds to the measured brightness in the 155–162 nm range multiplied 8.1 to scale it to the whole H_2 Lyman and Werner bands UV spectrum, based on a synthetic spectrum at 300 K without self-absorption (J. Gustin, personal communication, 2016). Near perijove, Juno-UVS acquired auroral observations during three sequences in the northern hemisphere (from 4:51 to 5:10 UT, from 09:51 to 11:02 UT, and from 11:51 to 12:02 UT spacecraft time) and one in the southern hemisphere (from 13:51 to 15:04 UT). Interruptions sometimes occurred during the data acquisition, either due to buffer saturation when particularly intense features came in sight or to high radiation levels, which might eventually lead the instrument to drop its voltage when the total detected counts is above the safety threshold. These interruptions create gaps in the swaths.

3. Juno-UVS Auroral Observations During PJ1

3.1. Morphology of the Aurorae

The unique vantage point of Juno, right above the poles, provides the first complete views of Jupiter's aurorae, including the nightside emissions. In the following description, letters refer to features in Figure 1, which provides a general view of the aurorae in the two hemispheres and the colored arrows to Figure 2, which shows the evolution of the morphology through time. In both figures, the red and green lines represent the footpaths of the Juno spacecraft obtained by projecting the position of Juno on Jupiter's surface along the magnetic field lines according to the VIP4 [*Connerney et al.*, 1998] and the VIPAL [*Hess et al.*, 2011] models, respectively. There are noticeable differences, and thus, those footpaths should be considered with care. Maps of both

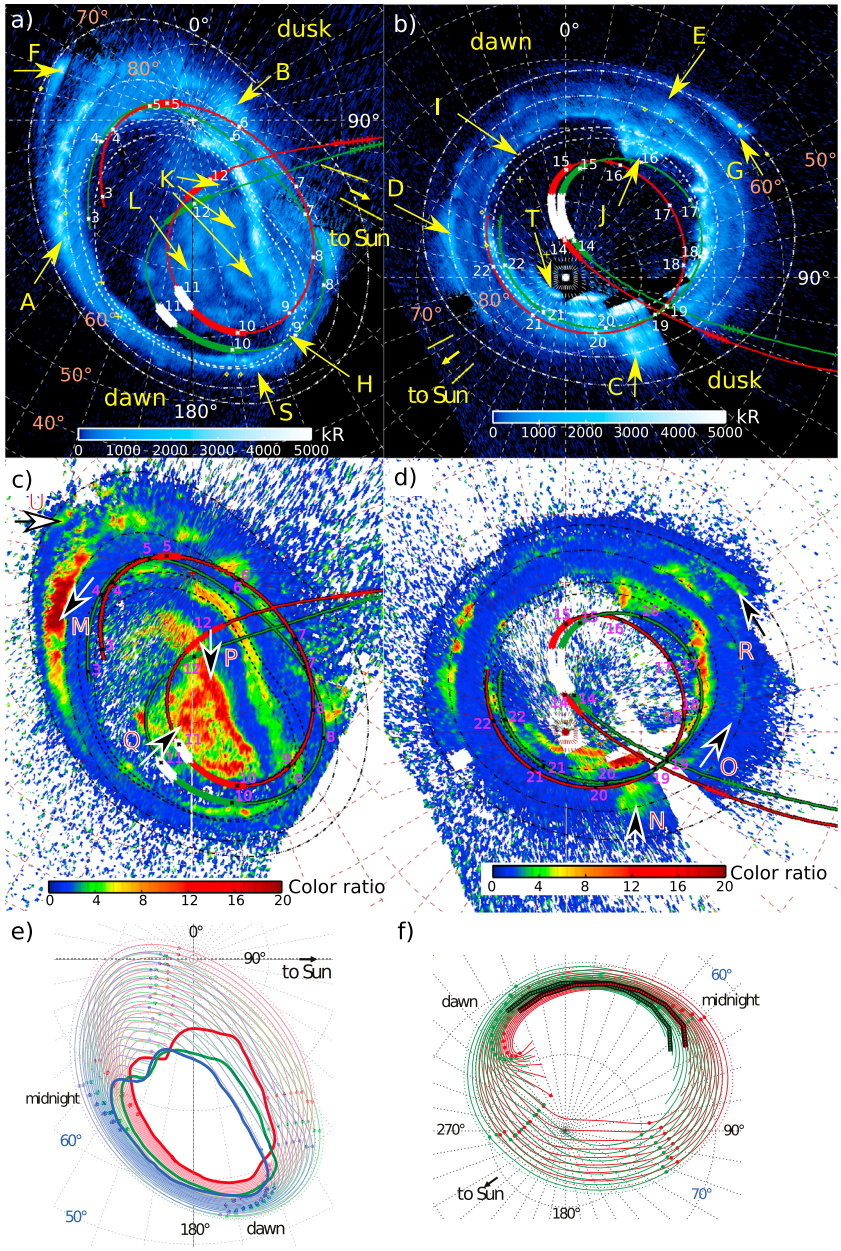

Figure 1. The top two panels are assemblages of polar projection of the data retrieved (a) between 10:46 and 11:01 for the northern hemisphere and (b) between 14:01 and 14:28 for the southern hemisphere. In the south, dark areas with sharp contour are due to data gaps. (c, d) Similar maps as in Figures 1a and 1b but for the color ratio. The green and red lines represent the Juno magnetic footprint according to the VIPAL [*Hess et al.*, 2011] and VIP4 [*Connerney et al.*, 1998] models, respectively. The line is slightly thicker when observations took place and the white stars highlight the footprint of Juno for the stripes used to build these particular maps. The two dash-dotted contours are the statistical fit of the Io footprint location and the Europa footpath according to the VIPAL model, while the two inner ones are the statistical location of the main emission observed by HST in 2007 for the compressed and expanded cases, respectively [*Bonfond et al.*, 2012]. The expected Io, Europa, and Ganymede footprint location at the beginning and at the end of the exposure are shown with diamonds. The sub-Juno position at the beginning and at the end of the exposure are shown with crosses. The description of the features highlighted by the letters is given in the text. (e) Ionospheric mapping contours in the north using the magnetic field mapping model of *Vogt et al.* [2015] for different internal magnetic field models: VIP4 (red), GAM [*Grodent et al.*, 2008] (blue), and VIPAL (green) and a subsolar longitude of 90° S_{III}. The thin lines represent the equatorial radial distance every 10 R_J from 20 R_J to 150 R_J. The thick line outlines the area open to the solar wind. (f) Similar to Figure 1e but for the south. The black and dashed lines are the projection of the statistical *X* line location from *Vogt et al.* [2010].

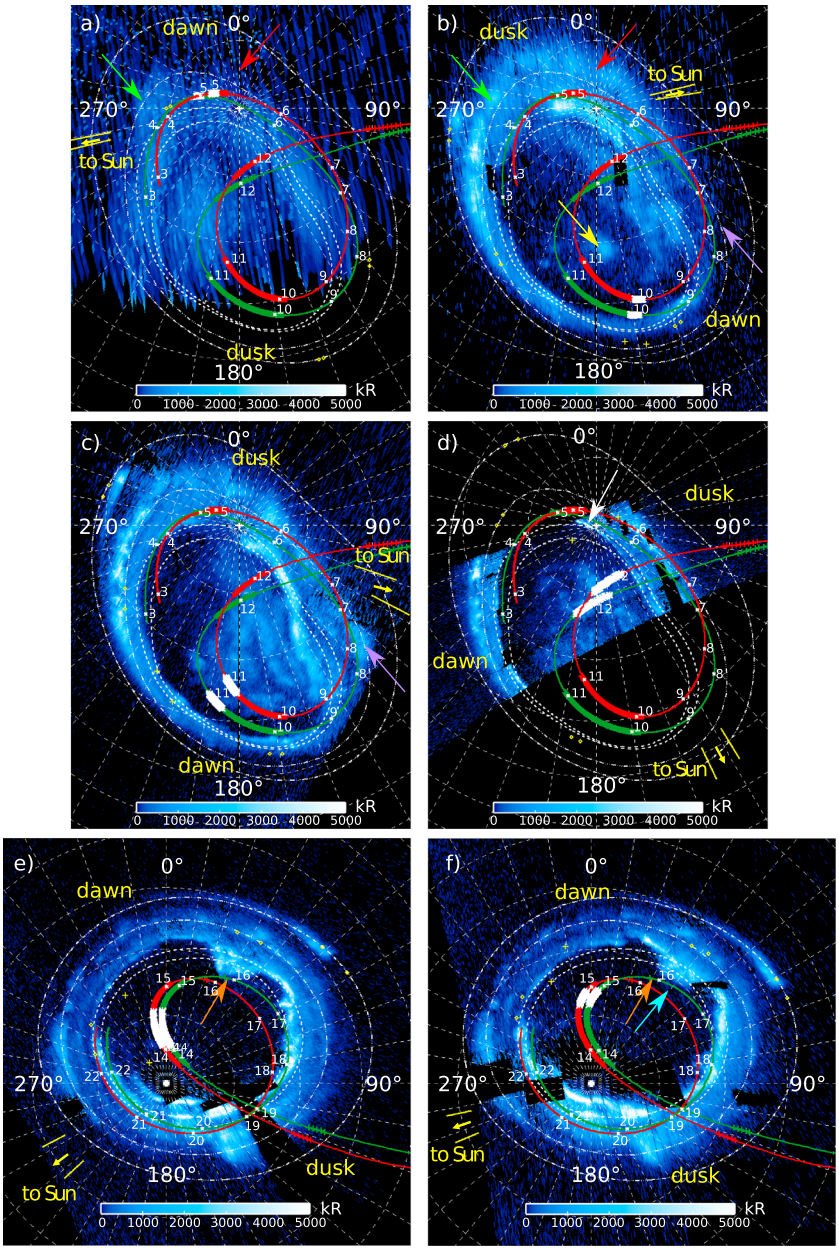

Figure 2. Polar projection of data acquired (a) between 04:54 and 05:00, (b) between 09:52 and 10:00, (c) between 10:46 and 11:01, (d) between 11:51 and 12:02, (e) between 14:01 and 14:28, and (f) between 14:34 and 14:52. Arrows of the same color highlight changes in the aurorae, and they point to the same location in System III.

northern and southern aurorae are oriented similarly, with 0° S_{III} at the top and 90° to the right, in order to facilitate interhemispheric comparisons. The view of the southern hemisphere corresponds to a view through the planet and is thus flipped east/west compared to what an observer above the pole would see. It should also be noted that the two views in Figure 1 are not simultaneous since ~3 h separate them. The northern map coadds data from 10:46 to 11:01 and the Sun's S_{III} longitude ranges from 109° to 118°. In the south, the map is a coaddition of data from 14:01 to 14:28 and the Sun's S_{III} longitude ranges from 228° to 243°. Figures 1c and 1d show maps of the color ratio between 155 and 162 nm wavelength range and 123 and 130 nm wavelength range [*Yung et al.*, 1982]. The color ratio method relies on the shape of the absorption cross section of CH_4 in the UV, which rapidly drops for wavelength larger than 140 nm. The amount of absorption depends on the altitude of the auroral emission relative to the hydrocarbon homopause. As a consequence, such measurements directly relate to the energy of the precipitating particles, since the more energetic the particles,

the deeper they penetrate and the stronger is the resulting CH_4 absorption. Unfortunately, the vertical distribution of CH_4 in the polar regions of Jupiter is poorly constrained by observations and the conversion from color ratio to electron energy is thus strongly model dependent. While most models agree that monoenergetic 100 keV electrons lead to a color ratio around 2 for a zenith angle of 60°, estimates for 500 keV electrons vary from 9 to 18 [*Gérard et al.*, 2014]. Furthermore, the conversion depends on the assumed energy distribution of the precipitating electrons (monoenergetic, Maxwellian, kappa, etc.) which should probably not be the same for the different components of the aurorae [*Gustin et al.*, 2016]. As a consequence, such a conversion requires some extensive discussions that we leave for future works.

Several aspects of the aurorae are remarkable on the images in Figure 1. First of all, both hemispheres show very intense outer emissions outside the main auroral oval. In the north, large stretches of emissions can be seen between 200° and 140° S_{III}, covering the entire nightside and duskside. The outer emissions are more evenly spread all around the pole in the south. Despite the time delay, magnetically conjugate counterparts of the most intense patches (A and B) in the north are still noticeable (D and E). Moreover, a bright patch of emission is present in the south at 140° S_{III}, without any counterpart in the north (C). In accordance with previous observations by *Dumont et al.* [2014], the outer emissions are most intense around the Europa footpath. If we consider the evolution of these emissions through time, the initial images acquired at large distance around 5:00 UT (Figure 2a) only show a limited patch of outer emissions (green arrow). Around 10:00 (Figure 2b), the outer emissions are considerably expanded in longitude (cf. red arrow) and brightened. This expansion in longitude continued, as a new bright patch appeared around local noon before 11:00 (purple arrow in Figure 2c).

The Io footprint can easily be identified on the images, including its major spots and its tail (Figure 1, F and G). On these polar projections, the apparent latitudinal brightness distribution of the spots and tail results from the combination of the viewing geometry and of the vertical extent of these emissions [*Bonfond et al.*, 2009; *Bonfond*, 2010]. The Europa footprint is located right within patches of outer emissions and cannot be isolated from it. Only one spot of the Ganymede footprint can be identified in the north (S), whereas the outer emissions in the south make the identification of the Ganymede footprint impossible. As for the Europa footprint, it is likely that the properties of the plasma related to the outer emissions are not favorable to bright footprints, because higher plasma densities at high latitude decrease the efficiency of the electron acceleration process [*Hess et al.*, 2013; *Bonfond et al.*, 2017].

As it is often the case when outer emissions are intense, the main emission (also called the main oval) is weak, irregular, and broken into patches [e.g., *Nichols et al.*, 2009]. A discontinuity of the main emission on the magnetic prenoon sector is also noticeable in both hemispheres [*Radioti et al.*, 2008a] (H and I). During the low-altitude flyby over the aurora, the main emission curtain appears to be as narrow as 175 km (white arrow on Figure 2d).

One of the most remarkable features observed by Juno-UVS during the first perijove observations is the large-scale protrusion into the polar region on the nightside flank of the main emission in the south (J). During the observations in the north, there was no counterpart of this feature in that hemisphere, neither fixed in local time nor fixed in System III. Actually, successive images of the same region show that it is strongly subcorotating. The cyan arrow in Figure 2f shows the new position of the protrusion while the orange one is fixed in a corotating frame. In HST images, the nightside is mostly hidden behind the limb and the only features identified in this region are barely discernible at the limb [*Grodent et al.*, 2003b; *Radioti et al.*, 2011]. Such features have been associated with Vasyliunas cycle nightside reconnections. The location of this protrusion is compatible with the projection of flux tubes located inside the reconnection *X* line [*Vogt et al.*, 2010], whose projections are represented as bold black lines on Figure 1f. This protrusion may be an early stage of what would later evolve as polar dawn spots [*Radioti et al.*, 2008b]; a process somewhat reminiscent of poleward boundary intensifications and streamers at Earth [e.g., *Nishimura et al.*, 2011].

Within the polar region, the dichotomy between the hemispheres is striking. In the south, a bright arc parallel to the main oval is present on the noon-to-dusk sector (T), with no clear counterpart in the former images of the north. In the north, the active region (K) shows intermittent polar auroral filaments and flares. These flares cover a large part of the active region and appear to abruptly stop at the border of the swirl region, similar to a case described in *Bonfond et al.* [2016] (see Movie S1 in the supporting information). Within the swirl region (L), emissions are patchy and relatively faint, except for a noticeable localized intensification that started shortly after 10:00 and lasted for ~10 min (yellow arrow in Figure 2b). While the difference between

the active and swirl regions blurs out in Figure 2c, the distinctive behaviors are still visible in the individual frames. On the other hand, apart from the protrusion and the arc described above, the entire polar regions appear nearly devoid of any emission in the south.

3.2. Color Ratio

A comparison between the brightness maps and the color ratio (CR) maps provides additional information. The Io footprint is a relatively bright feature (Figure 1, F and G), but its color ratio is low (R and U). The front of Io's northern footprint, which would correspond to a transhemispheric electron beam spot, is more absorbed. It indicates that this spot is formed at lower altitude than the other spots and tail, in accordance with previous HST observations above the limb [*Bonfond*, 2010]. In the south, only the polarmost part of it, which actually corresponds to the bottom of the vertical profile in the atmosphere, shows some signature of methane abortion (R, CR $\simeq$ 4), again in accordance with previous observations from HST [*Gérard et al.*, 2002; *Bonfond et al.*, 2009; *Gérard et al.*, 2016].

In the north, the large patch of outer emissions on the nightside is strongly absorbed (M), indicative of precipitation of high-energy particles. Its southern counterpart observed 3 h later is much less absorbed, but it is not clear whether this is due to temporal effects or to magnetic field asymmetries. Areas covered by more diffuse emissions, as the one noted (O) in the southern hemisphere, for example, appear to have a much lower color ratio. Interestingly, for some of the brightest features of the outer emissions, such as the one marked with a C, the color ratio peak does not correspond to the brightness peak but is found downstream relative to the rotation of the plasma around Jupiter. In Figure 1, the arrows close to the letters C and N point to the exact same location, but the color ratio peak is $\sim$10° left of the brightness peak. The most likely interpretation for these patches are that they are signatures of plasma injections from the middle magnetosphere to the inner magnetosphere [*Mauk et al.*, 2002; *Dumont et al.*, 2014]. Once a flux tube filled with hot plasma is suddenly injected toward the planet, the particles of various energy experience a differential drift due to the gradients and curvatures of the magnetic field. Hence, in situ energetic electron measurements of plasma injections show enhancements of the lower-energy electron flux before enhancement of the higher-energy electron flux [*Mauk et al.*, 2002]. The shift described here would be the auroral counterpart of this differential drift. Our observation would then be a compelling evidence that these features are indeed related to the radial transport of plasma within the magnetosphere.

The most striking addition of the color ratio map is the strongly absorbed mussel shell-shaped region corresponding to the swirl region. For example, the remarkable spot Q and the arc P have only faint counterpart in the brightness map, compared to the main emission. In the CR map, the arc P appears as a boundary between two regions. Indeed, the shape, location, and area of this region resemble those of the fixed Dark Polar Region in the H_3^+ Doppler shift observations [*Stallard et al.*, 2003] and the region open to the solar wind according to the flux equivalence model of *Vogt et al.* [2011, 2015] (see Figure 1e). Should this region actually correspond to open field lines, then it remains to explain why it can be occasionally filled with auroral emission while equivalent regions are essentially devoid of emission both at Earth and at Saturn.

3.3. Brightness Along the Juno Footpath

Figure 3 shows the brightness profiles along the Juno magnetic footpath, which are expected to be connected with the energetic particle population measured in situ [*Mauk et al.*, 2017]. Depending on the magnetic field model in use, i.e., either VIP4 [*Connerney et al.*, 1998] or VIPAL [*Hess et al.*, 2011], the results are significantly different. These differences reflect the current uncertainty concerning the magnetic field of Jupiter. Hence, the profiles shown here should be considered with caution. Furthermore, as demonstrated in section 3.1, the aurorae change with time. The different maps of Figure 2 have been used for the different time intervals separated with the dashed red lines. However, even by using the closest map available, the precipitating plasma population at the time of the Juno-UVS observation may not be the same as when the spacecraft was crossing the field lines mapping to a given location.

In the north, Juno entered the outer emission region between 03:00 and 04:00 and remained there until $\sim$09:00. Depending on the model, Juno either crossed the beginning of the dawn branch of the main emission (VIPAL) or remained in the dim discontinuity region (VIP4). It remained in the dark region until approximately 11:00. Juno's footprint then entered the swirl region around noon and crossed the main emission between 12:06 (VIP4) and 12:08 (VIPAL) and some outer emission shortly before (VIP4) or after (VIPAL) 12:12. It should be noted that the last and larger brightness peak is related with these outer emissions, not with the main emission crossing.

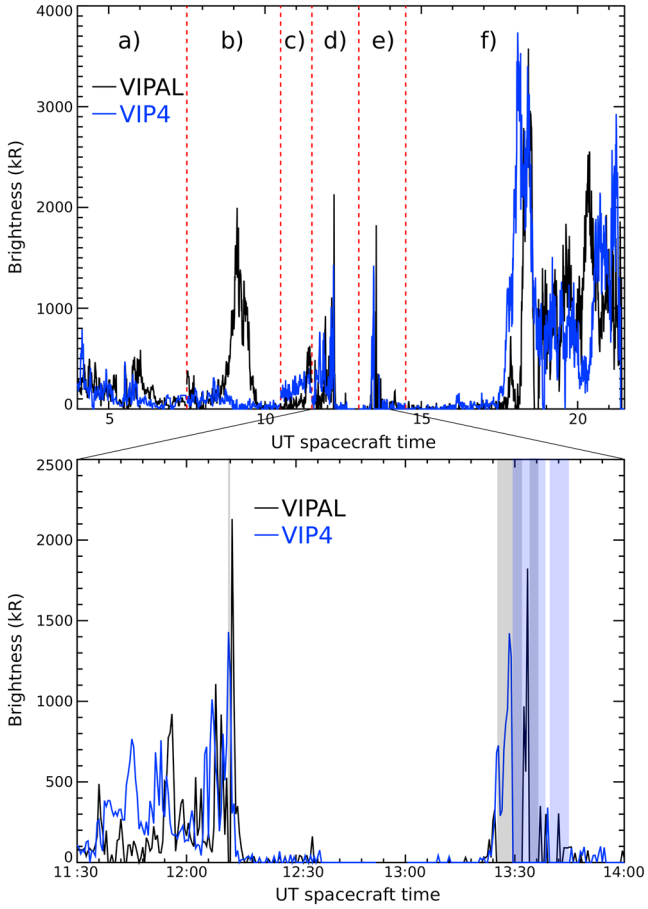

Figure 3. Brightness profiles along the Juno footpath according to the VIP4 (blue) and VIPAL (black) magnetic field models, respectively. (top) The whole sequence from 4:00 UT to 21:30 UT. Because the aurorae evolved with time, the polar map (from Figure 2) used to extract the profile are indicated with the appropriate letter. (bottom) A zoom centered on the perijove time, the first half corresponding to the north and the end of the sequence to the south. The shaded areas correspond to regions where no data were acquired at the time of the map acquisition. The last brightness peak in the north corresponds to a brightness peak in the outer emission rather than the main emission.

In the south, Juno's footprint crossed the main emission around 13:30, right after getting across a rather intense area of outer emissions. Unfortunately, data gaps prevent us to know exactly what happened during this crossing. It may have encountered the short parallel arc (noted M in Figure 1) or it may have just missed it. The next couple of hours were spent in the featureless polar region, only to brush a small protrusion and cross the main oval again around 19:00. It then spent ~2 h within the outer emission region, skimming the main oval before crossing it one last time around 21:30. It should however be noted that the last Juno-UVS observation took place shortly before 15:00 and that the evolution of the different UV auroral features after this time is unknown.

4. Discussion and Conclusions

Many features observed by Juno-UVS during this first set of high spatial resolution observations are consistent with previous observations, e.g., with the Hubble Space Telescope. However, the duration, spatial resolution, and spectral resolution of these observations open new insight into the Jovian aurorae.

Louarn et al. [2014] showed that there is a relationship between (1) large-scale energetic events likely associated with reconnection at the edge of the plasma sheet on the nightside and (2) new energetic electron injections within the middle magnetosphere. The auroral observations carried out by Juno-UVS during its first perijove around Jupiter appears to concur with this view and may even provide some precisions. These successive sets of images acquired over a jovian rotation show the formation and the subsequent spread of intense outer emissions. While the brightest outer emission features appear on the nightside in the north, the new

features likely formed on the dayside and then corotate. The observed shifts between precipitating electrons of different energy, in accordance with the differential drift expected in plasma injections, indicated that at least parts of these outer emissions are caused by injected particles which are supposedly part of large-scale radial plasma transport. If the events reported above are correctly interpreted and if they are indeed causally related, they suggest that, during PJ1, large-scale injections preceded a large-scale tail reconnection. Eighty Jovian radii (R_J) typically separate the radial distance of injections (10 R_J) from the radial distance of the reconnection X line (90 R_J). The first injection signature was observed at dawn around 05:00, and the protrusion was first observed at midnight around 13:00. A connection between these two sites would thus involve radial propagation speeds around 200 km/s, which is close to the highest estimates of the radial transport speed at such distances in the Jovian magnetosphere (60–200 km/s) [*Bagenal and Delamere*, 2011]. A possible scenario could be that a parcel of cold plasma could suddenly migrate outward owing to large-scale interchange instability, rotate around Jupiter for three fourths of a full rotation and then be released in the magnetotail as a plasmoid after reconnection. This radial propagation speed is also quite similar to estimates of the Alfvén velocity between Europa (∼160 km/s [*Kivelson et al.*, 2004]) and the lobes of the magnetotail (∼350 km/s [*Cowley et al.*, 2015]). An alternative scenario could be that large-scale plasma injections in the middle magnetosphere generate significant disturbances in the field topology propagating outward around the Alfvén speed and then trigger reconnection in the tail. If plasma injections indeed precede Vasyliunas-type tail reconnection, then a similar chain of events may also explain the simultaneous observation of large outer emission blobs, which last for several hours [*Dumont et al.*, 2014], together with a bright polar dawn spot, which typically last for a few tens of minutes [*Radioti et al.*, 2008a], as reported by *Gray et al.* [2016]. More observations are however required to confirm this still speculative scenario. Among others, it remains to be verified if the large protrusion observed in the south is actually related to tail reconnection.

The differences observed in the northern and southern polar regions are puzzling. Future simultaneous observations of both poles from Juno and HST will clarify whether this is a temporal or a hemispheric effect. Differences between the brightness at different wavelengths is also striking in the northern polar region. In color ratio maps, a well-defined region clearly emerges and it resembles the size and shape of the open field line region expected from the flux mapping model of *Vogt et al.* [2015].

Acknowledgments

We are grateful to NASA and contributing institutions which have made the Juno mission possible. This work was funded by NASA's New Frontiers Program for Juno via contract with the Southwest Research Institute. B.B., D.G., A.R. and J.-C.G. were supported by the PRODEX program managed by ESA in collaboration with the Belgian Federal Science Policy Office. M.F.V. was supported by the National Science Foundation under award 1524651. The research at the University of Iowa was supported by NASA through contract 699041X with Southwest Research Institute. The data included herein are on schedule to be archived in NASA's Planetary Data System.

References

Badman, S. V., et al. (2016), Weakening of Jupiter's main auroral emission during January 2014, *Geophys. Res. Lett.*, *43*, 988–997, doi:10.1002/2015GL067366.

Bagenal, F., and P. A. Delamere (2011), Flow of mass and energy in the magnetospheres of Jupiter and Saturn, *J. Geophys. Res.*, *116*, A05209, doi:10.1029/2010JA016294.

Bonfond, B. (2010), The 3-D extent of the Io UV footprint on Jupiter, *J. Geophys. Rese.*, *115*, A09217, doi:10.1029/2010JA015475.

Bonfond, B. (2012), When moons create aurora: The satellite footprints on giant planets, in *Auroral Phenomenology and Magnetospheric Processes: Earth And Other Planets, Geophys. Monogr. Ser.*, vol. 197, edited by A. Keiling et al., pp. 133–140, AGU, Washington, D. C., doi:10.1029/2011GM001169

Bonfond, B., D. Grodent, J.-C. Gérard, A. Radioti, V. Dols, P. A. Delamere, and J. T. Clarke (2009), The Io UV footprint: Location, inter-spot distances and tail vertical extent, *J. Geophys. Res.*, *114*, A07224, doi:10.1029/2009JA014312.

Bonfond, B., M. F. Vogt, J.-C. Gérard, D. Grodent, A. Radioti, and V. Coumans (2011), Quasi-periodic polar flares at Jupiter: A signature of pulsed dayside reconnections?, *Geophys. Res. Lett.*, *380*, L02104, doi:10.1029/2010GL045981.

Bonfond, B., D. Grodent, J.-C. Gérard, T. Stallard, J. T. Clarke, M. Yoneda, A. Radioti, and J. Gustin (2012), Auroral evidence of Io's control over the magnetosphere of Jupiter, *Geophys. Res. Lett.*, *39*, L01105, doi:10.1029/2011GL050253.

Bonfond, B., J. Gustin, J. C. Gérard, D. Grodent, A. Radioti, B. Palmaerts, S. V. Badman, K. K. Khurana, and C. Tao (2015), The far-ultraviolet main auroral emission at Jupiter—Part 2: Vertical emission profile, *Ann. Geophys.*, *33*, 1211–1219.

Bonfond, B., D. Grodent, S. V. Badman, J.-C. Gérard, and A. Radioti (2016), Dynamics of the flares in the active polar region of Jupiter, *Geophys. Res. Lett.*, *43*, 11,963–11,970, doi:10.1002/2016GL071757.

Bonfond, B., D. Grodent, S. Badman, J. Saur, J.-C. Gérard, and A. Radioti (2017), Similarity of the jovian satellite footprints: Spots multiplicity and dynamics, *Icarus*, doi:10.1016/j.icarus.2017.01.009.

Connerney, J. E. P., R. Baron, T. Satoh, and T. Owen (1993), Images of excited H_3^+ at the foot of the Io flux tube in Jupiter's atmosphere, *Science*, *262*, 1035–1038.

Connerney, J. E. P., M. H. Acuña, N. F. Ness, and T. Satoh (1998), New models of Jupiter's magnetic field constrained by the Io flux tube footprint, *J. Geophys. Res.*, *103*, 11,929–11,940, doi:10.1029/97JA03726.

Cowley, S. W. H., and E. J. Bunce (2001), Origin of the main auroral oval in Jupiter's coupled magnetosphere-ionosphere system, *Planet. Space Sci.*, *49*, 1067–1088, doi:10.1016/S0032-0633(00)00167-7.

Cowley, S. W. H., J. D. Nichols, and C. M. Jackman (2015), Down-tail mass loss by plasmoids in Jupiter's and Saturn's magnetospheres, *J. Geophys. Res. Space Physics*, *120*, 6347–6356, doi:10.1002/2015JA021500.

Davis, M. W., G. R. Gladstone, T. K. Greathouse, D. C. Slater, M. H. Versteeg, K. B. Persson, G. S. Winters, S. C. Persyn, and J. S. Eterno (2011), Radiometric performance results of the Juno ultraviolet spectrograph (Juno-UVS), in *UV/Optical/IR Space Telescopes and Instruments: Innovative Technologies and Concepts V, Soc. of Photo-Opt. Instrum. Eng. (SPIE) Conf. Ser., Proc. SPIE*, vol. 8146, edited by H. A. MacEwen and J. B. Breckinridge, p. 814604, SPIE, San Diego, Calif., doi:10.1117/12.894274.

Dumont, M., D. Grodent, A. Radioti, B. Bonfond, and J.-C. Gérard (2014), Jupiter's equatorward auroral features: Possible signatures of magnetospheric injections, *J. Geophys. Res. Space Physics*, *119*, 10068, doi:10.1002/2014JA020527.

Gérard, J.-C., J. Gustin, D. Grodent, P. Delamere, and J. T. Clarke (2002), Excitation of the FUV Io tail on Jupiter: Characterization of the electron precipitation, *J. Geophys. Res.*, *107*(A11), 1394, doi:10.1029/2002JA009410.

Gérard, J.-C., B. Bonfond, D. Grodent, A. Radioti, J. T. Clarke, G. R. Gladstone, J. H. Waite, D. Bisikalo, and V. I. Shematovich (2014), Mapping the electron energy in Jupiter's aurora: Hubble spectral observations, *J. Geophys. Res. Space Physics*, *119*, 9072–9088, doi:10.1002/2014JA020514.

Gérard, J.-C., B. Bonfond, D. Grodent, and A. Radioti (2016), The color ratio-intensity relation in the Jovian aurora: Hubble observations of auroral components, *Planet. Space Sci.*, *131*, 14–23, doi:10.1016/j.pss.2016.06.004.

Gladstone, G. R., et al. (2014), The ultraviolet spectrograph on NASA's Juno mission, *Space Sci. Rev.*, doi:10.1007/s11214-014-0040-z.

Gray, R. L., S. V. Badman, B. Bonfond, T. Kimura, H. Misawa, J. D. Nichols, M. F. Vogt, and L. C. Ray (2016), Auroral evidence of radial transport at Jupiter during January 2014, *J. Geophys. Res. Space Physics*, *121*, 9972–9984, doi:10.1002/2016JA023007.

Greathouse, T. K., G. R. Gladstone, M. W. Davis, D. C. Slater, M. H. Versteeg, K. B. Persson, B. C. Walther, G. S. Winters, S. C. Persyn, and J. S. Eterno (2013), Performance results from in-flight commissioning of the Juno Ultraviolet Spectrograph (Juno-UVS), in *UV, X-Ray, and Gamma-Ray Space Instrumentation for Astronomy XVIII, Proc. SPIE*, vol. 8859, edited by O. H. Siegmund, p. 88590T, SPIE, San Diego, Calif., doi:10.1117/12.2024537.

Grodent, D. (2015), A brief review of ultraviolet auroral emissions on giant Planets, *Space Sci. Rev.*, *187*, 23–50, doi:10.1007/s11214-014-0052-8.

Grodent, D., J. T. Clarke, J. Kim, J. H. Waite, and S. W. H. Cowley (2003a), Jupiter's main auroral oval observed with HST-STIS, *J. Geophys. Res.*, *108*(A11), 1389, doi:10.1029/2003JA009921.

Grodent, D., J. T. Clarke, J. H. Waite, S. W. H. Cowley, J.-C. Gérard, and J. Kim (2003b), Jupiter's polar auroral emissions, *J. Geophys. Res.*, *108*(A10), 1366, doi:10.1029/2003JA010017.

Grodent, D., B. Bonfond, J.-C. Gérard, A. Radioti, J. Gustin, J. T. Clarke, J. Nichols, and J. E. P. Connerney (2008), Auroral evidence of a localized magnetic anomaly in Jupiter's northern hemisphere, *J. Geophys. Res.*, *113*, A09201, doi:10.1029/2008JA013185.

Gustin, J., D. Grodent, L. C. Ray, B. Bonfond, E. J. Bunce, J. D. Nichols, and N. Ozak (2016), Characteristics of north Jovian aurora from STIS FUV spectral images, *Icarus*, *268*, 215–241, doi:10.1016/j.icarus.2015.12.048.

Hess, S. L. G., B. Bonfond, P. Zarka, and D. Grodent (2011), Model of the Jovian magnetic field topology constrained by the Io auroral emissions, *J. Geophys. Res.*, *116*, A05217, doi:10.1029/2010JA016262.

Hess, S. L. G., B. Bonfond, and P. A. Delamere (2013), How could the Io footprint disappear?, *Planet. Space Sci.*, *89*, 102–110, doi:10.1016/j.pss.2013.08.014.

Hill, T. W. (2001), The Jovian auroral oval, *J. Geophys. Res.*, *106*, 8101–8108, doi:10.1029/2000JA000302.

Kivelson, M. G., F. Bagenal, W. S. Kurth, F. M. Neubauer, C. Paranicas, and J. Saur (2004), Magnetospheric interactions with satellites, in *Jupiter. The Planet, Satellites and Magnetosphere*, edited by F. Bagenal, T. E. Dowling, and W. B. McKinnon, pp. 513–536, Cambridge Univ. Press, Cambridge, U. K.

Louarn, P., C. P. Paranicas, and W. S. Kurth (2014), Global magnetodisk disturbances and energetic particle injections at Jupiter, *J. Geophys. Res. Space Physics*, *119*, 4495–4511, doi:10.1002/2014JA019846.

Mauk, B. H., J. T. Clarke, D. Grodent, J. H. Waite, C. P. Paranicas, and D. J. Williams (2002), Transient aurora on Jupiter from injections of magnetospheric electrons, *Nature*, *415*, 1003–1005.

Mauk, B. H., et al. (2017), Juno observations of energetic charged particles over Jupiters polar regions: Analysis of mono and bi-directional electron beams, *Geophys. Res. Lett.*, doi:10.1002/2016GL072286, in press.

Nichols, J. D., E. J. Bunce, J. T. Clarke, S. W. H. Cowley, J.-C. Gérard, D. Grodent, and W. R. Pryor (2007), Response of Jupiter's UV auroras to interplanetary conditions as observed by the Hubble Space Telescope during the Cassini flyby campaign, *J. Geophys. Res.*, *112*, A02203, doi:10.1029/2006JA012005.

Nichols, J. D., J. T. Clarke, J. C. Gérard, D. Grodent, and K. C. Hansen (2009), Variation of different components of Jupiter's auroral emission, *J. Geophys. Res.*, *114*, A06210, doi:10.1029/2009JA014051.

Nishimura, Y., L. R. Lyons, V. Angelopoulos, T. Kikuchi, S. Zou, and S. B. Mende (2011), Relations between multiple auroral streamers, pre-onset thin arc formation, and substorm auroral onset, *J. Geophys. Res.*, *116*, A09214, doi:10.1029/2011JA016768.

Radioti, A., J.-C. Gérard, D. Grodent, B. Bonfond, N. Krupp, and J. Woch (2008a), Discontinuity in Jupiter's main auroral oval, *J. Geophys. Res.*, *113*, A01215, doi:10.1029/2007JA012610.

Radioti, A., D. Grodent, J.-C. Gérard, B. Bonfond, and J. T. Clarke (2008b), Auroral polar dawn spots: Signatures of internally driven reconnection processes at Jupiter's magnetotail, *Geophys. Res. Lett.*, *35*, L03104, doi:10.1029/2007GL032460.

Radioti, A., A. T. Tomás, D. Grodent, J.-C. Gérard, J. Gustin, B. Bonfond, N. Krupp, J. Woch, and J. D. Menietti (2009), Equatorward diffuse auroral emissions at Jupiter: Simultaneous HST and Galileo observations, *Geophys. Res. Lett.*, *36*, L07101, doi:10.1029/2009GL037857.

Radioti, A., D. Grodent, J.-C. Gérard, M. F. Vogt, M. Lystrup, and B. Bonfond (2011), Nightside reconnection at Jupiter: Auroral and magnetic field observations from 26 July 1998, *J. Geophys. Res.*, *116*, A03221, doi:10.1029/2010JA016200.

Stallard, T. S., S. Miller, S. W. H. Cowley, and E. J. Bunce (2003), Jupiter's polar ionospheric flows: Measured intensity and velocity variations poleward of the main auroral oval, *Geophys. Res. Lett.*, *30*(5), 1221, doi:10.1029/2002GL016031.

Vogt, M. F., M. G. Kivelson, K. K. Khurana, S. P. Joy, and R. J. Walker (2010), Reconnection and flows in the Jovian magnetotail as inferred from magnetometer observations, *J. Geophys. Res.*, *115*, A06219, doi:10.1029/2009JA015098.

Vogt, M. F., M. G. Kivelson, K. K. Khurana, R. J. Walker, B. Bonfond, D. Grodent, and A. Radioti (2011), Improved mapping of Jupiter's auroral features to magnetospheric sources, *J. Geophys. Res.*, *116*, A03220, doi:10.1029/2010JA016148.

Vogt, M. F., E. J. Bunce, M. G. Kivelson, K. K. Khurana, R. J. Walker, A. Radioti, B. Bonfond, and D. Grodent (2015), Magnetosphere-ionosphere mapping at Jupiter: Quantifying the effects of using different internal field models, *J. Geophys. Res. Space Physics*, *120*, 2584–2599, doi:10.1002/2014JA020729.

Waite, J. H., et al. (2001), An auroral flare at Jupiter, *Nature*, *410*, 787–789.

Yung, Y. L., G. R. Gladstone, K. M. Chang, J. M. Ajello, and S. K. Srivastava (1982), H_2 fluorescence spectrum from 1200 to 1700 A by electron impact—Laboratory study and application to Jovian aurora, *Astrophys. J.*, *254*, L65–L69, doi:10.1086/183757.